Video Article

Quantification of Hydrogen Concentrations in Surface and Interface Layers and Bulk Materials through Depth Profiling with Nuclear Reaction Analysis

Markus Wilde[1], Satoshi Ohno[1], Shohei Ogura[1], Katsuyuki Fukutani[1], Hiroyuki Matsuzaki[2]

[1]Institute of Industrial Science, The University of Tokyo

[2]Micro Analysis Laboratory, Tandem accelerator, The University Museum, The University of Tokyo

Correspondence to: Markus Wilde at wilde@iis.u-tokyo.ac.jp

URL: https://www.jove.com/video/53452
DOI: doi:10.3791/53452

Keywords: Engineering, Issue 109, Hydrogen quantitation, depth profiling, surface hydrogen, bulk hydrogen, interface hydrogen, nuclear reaction analysis, ion beam analysis

Date Published: 3/29/2016

Citation: Wilde, M., Ohno, S., Ogura, S., Fukutani, K., Matsuzaki, H. Quantification of Hydrogen Concentrations in Surface and Interface Layers and Bulk Materials through Depth Profiling with Nuclear Reaction Analysis. *J. Vis. Exp.* (109), e53452, doi:10.3791/53452 (2016).

Abstract

Nuclear reaction analysis (NRA) via the resonant $^{1}H(^{15}N,\alpha\gamma)^{12}C$ reaction is a highly effective method of depth profiling that quantitatively and non-destructively reveals the hydrogen density distribution at surfaces, at interfaces, and in the volume of solid materials with high depth resolution. The technique applies a ^{15}N ion beam of 6.385 MeV provided by an electrostatic accelerator and specifically detects the ^{1}H isotope in depths up to about 2 µm from the target surface. Surface H coverages are measured with a sensitivity in the order of ~10^{13} cm^{-2} (~1% of a typical atomic monolayer density) and H volume concentrations with a detection limit of ~10^{18} cm^{-3} (~100 at. ppm). The near-surface depth resolution is 2-5 nm for surface-normal ^{15}N ion incidence onto the target and can be enhanced to values below 1 nm for very flat targets by adopting a surface-grazing incidence geometry. The method is versatile and readily applied to any high vacuum compatible homogeneous material with a smooth surface (no pores). Electrically conductive targets usually tolerate the ion beam irradiation with negligible degradation. Hydrogen quantitation and correct depth analysis require knowledge of the elementary composition (besides hydrogen) and mass density of the target material. Especially in combination with ultra-high vacuum methods for *in-situ* target preparation and characterization, $^{1}H(^{15}N,\alpha\gamma)^{12}C$ NRA is ideally suited for hydrogen analysis at atomically controlled surfaces and nanostructured interfaces. We exemplarily demonstrate here the application of ^{15}N NRA at the MALT Tandem accelerator facility of the University of Tokyo to (1) quantitatively measure the surface coverage and the bulk concentration of hydrogen in the near-surface region of a H_2 exposed Pd(110) single crystal, and (2) to determine the depth location and layer density of hydrogen near the interfaces of thin SiO_2 films on Si(100).

Video Link

The video component of this article can be found at https://www.jove.com/video/53452/

Introduction

The ubiquity of hydrogen as an impurity or as a constituent of a vast variety of materials and the wealth of hydrogen-induced interaction phenomena make revealing the hydrogen distribution in the near-surface region and at buried interfaces of solids an important task in many areas of engineering and fundamental material science. Prominent contexts include studies of hydrogen absorption in storage and purification materials for hydrogen energy applications, fuel cell, photo-, and hydrogenation catalysis, hydrogen retention and embrittlement in nuclear and fusion reactor engineering, hydrogen-induced surfactant effects in epitaxial growth fabrication and hydrogen-related electrical reliability issues in semiconductor device technology.

Despite its omnipresence and simple atomic structure, the quantitative detection of hydrogen poses analytical challenges. As hydrogen contains only a single electron, otherwise versatile elemental analysis by electron spectroscopy is rendered ineffective. Common hydrogen detection methods through mass analytical, optical, or nuclear resonance techniques such as metallurgical fusion, thermal desorption, infrared absorption or NMR spectroscopy are principally insensitive to the depth location of hydrogen. This precludes, *e.g.*, discriminating between surface-adsorbed and bulk-absorbed hydrogen which differ substantially in their physical and chemical material interactions, and their distinction therefore becomes increasingly important for the analysis of nanostructured materials that comprise small volumes and large surface areas. Hydrogen profiling by secondary ion mass spectroscopy, although providing depth-resolved quantitative H concentrations, is equally destructive to the analyzed target as metallurgical fusion, and sputtering effects may render the depth information obtained near the surface unreliable.

Nuclear reaction analysis with the narrow energy resonance (E_{res}) of the $^{1}H(^{15}N,\alpha\gamma)^{12}C$ reaction at 6.385 MeV[1-3], on the other hand, combines the advantages of non-destructive hydrogen quantitation with high depth resolution in the order of a few nanometers near the surface. The method determines surface H coverages with a sensitivity in the order of 10^{13} cm^{-2} (~1% of a typical atomic monolayer density). Hydrogen concentrations in the interior of materials can be assessed with a detection limit of several 10^{18} cm^{-3} (~100 at. ppm) and a probing depth range of about 2 µm. The near-surface depth resolution is routinely 2-5 nm in surface-normal incidence of the ^{15}N ion beam onto the analyzed target. In surface-grazing incidence geometries, the resolution can be enhanced further to values below 1 nm. See Ref. 3 for a detailed account.

These capabilities have proven $^{1}H(^{15}N,\alpha\gamma)^{12}C$ NRA as a powerful technique to elucidate the static and dynamic behavior of hydrogen at surfaces and interfaces in a large variety of processes and materials[3]. Established by Lanford[4] in 1976, ^{15}N NRA was first used predominantly to quantitatively determine volume H concentrations in bulk materials and thin films. Among other purposes, the absolute hydrogen concentrations obtained through ^{15}N NRA have been used to calibrate other, not directly quantitative, hydrogen detection techniques[5,6]. Also ^{15}N NRA hydrogen profiling in targets with well-defined interfaces in layered thin film structures has been described[7-10]. More recently, much progress has been achieved in studying hydrogen in the near-surface region of chemically clean and structurally well-defined targets by combining ^{15}N NRA with surface analytical ultra-high vacuum (UHV) instrumentation to prepare atomically controlled surfaces *in situ* for the H analysis[3].

By quantifying the hydrogen coverage on single crystal surfaces, NRA has contributed significantly to the current microscopic understanding of hydrogen adsorption phases on many materials. $^{1}H(^{15}N,\alpha\gamma)^{12}C$ NRA is furthermore the only experimental technique to directly measure the zero-point vibrational energy of surface-adsorbed H atoms[11], *i.e.*, it can reveal the quantum-mechanical vibrational motion of adsorbed H atoms in the direction of the incident ion beam. Through the capability of nanometer-scale discrimination between surface-adsorbed and bulk-absorbed H, ^{15}N NRA can provide valuable insight into the hydrogen ingress through material surfaces, such as relevant to mineral hydration dating[12] or for observing hydride nucleation underneath surfaces of H-absorbing metals[13-15]. High-resolution ^{15}N NRA applications have demonstrated the potential to detect sub-monolayer thickness variations of adlayers[16] and to distinguish surface-adsorbed from volume-absorbed hydrogen in Pd nanocrystals[17]. The combination with thermal desorption spectroscopy (TDS) allows for unambiguous identifications of H_2 thermal desorption features and for the depth-resolved assessment of the thermal stability of adsorbed and absorbed hydrogen states against desorption and diffusion[13,15,18]. Due to its non-destructive nature and high depth resolution $^{1}H(^{15}N,\alpha\gamma)^{12}C$ NRA is also the ideal method to detect hydrogen buried at intact interfaces, which allows for studying hydrogen trapping at metal/metal[19-22] and metal/semiconductor interfaces[16,23-25] and for tracking hydrogen diffusion in stacked thin film systems[9]. By directly visualizing hydrogen redistribution phenomena between interfaces of SiO_2/Si-based metal-oxide-semiconductor (MOS) structures that relate to electrical device degradation, NRA has made particularly valuable contributions to device reliability research[26].

The hydrogen detection principle in NRA is to irradiate the analyzed target with a ^{15}N ion beam of at least E_{res}=6.385 MeV to induce the resonant $^{1}H(^{15}N,\alpha\gamma)^{12}C$ nuclear reaction between ^{15}N and ^{1}H in the material. This reaction releases characteristic γ-rays of 4.43 MeV that are measured with a scintillation detector nearby the sample. The γ-yield is proportional to the H concentration in a certain depth of the target. Normalizing this signal by the number of incident ^{15}N ions converts it into absolute H density after the γ-detection system has been calibrated with a standard target of known H concentration. ^{15}N ions incident at E_{res} can react with hydrogen on the target surface. The concentration of buried hydrogen is measured with ^{15}N ions incident at energies (E_i) above E_{res}. Inside the target material, the ^{15}N ions suffer energy loss due to electronic stopping. This effect provides the high depth resolution, because the $^{1}H(^{15}N,\alpha\gamma)^{12}C$ nuclear reaction resonance has a very narrow width (Lorentzian width parameter Γ = 1.8 keV) and the stopping power of materials for 6.4 MeV ^{15}N ranges between 1-4 keV/nm, so that the passage of the ^{15}N ion through only a few atomic layers is sufficient to shift its energy outside the resonance window. Thus, the resonant reaction detects buried H at $E_i > E_{res}$ in a probing depth $d=(E_i-E_{res})/S$, where S is the electronic stopping power of the analyzed material[3].

By measuring the γ-yield while scanning the incident ^{15}N ion energy in small increments, one obtains a nuclear reaction excitation curve that contains the density-depth distribution of hydrogen in the target. In this excitation curve (γ-yield vs. ^{15}N energy), the actual H depth distribution is convolved with the NRA instrumental function that adds a predominantly Gaussian broadening and is the main limitation for the depth resolution[3]. At the surface (*i.e.*, at $E_i = E_{res}$) the Gaussian width is dominated by a Doppler Effect due to zero-point vibration of the H atoms against the target surface.[11,27,28] The yield curve of buried hydrogen detected at $E_i > E_{res}$ is affected by an additional Gaussian broadening component due to random ^{15}N ion energy straggling inside the target. The straggling width increases in proportion to the square root of the ion trajectory length in the material [29,30] and becomes the dominant resolution limiting factor above probing depths of 10-20 nm.

To demonstrate a few very typical hydrogen profiling applications with ^{15}N NRA, we here exemplarily describe (1) the quantitative evaluation of the surface H coverage and of the bulk-absorbed hydrogen concentration in a H_2 exposed palladium (Pd) single crystal, and (2) the evaluation of the depth location and hydrogen layer densities at buried interfaces of SiO_2/Si(100) stacks. The NRA measurements are performed at the MALT 5 MV van-de-Graaf tandem accelerator[31] of the University of Tokyo, which delivers a highly stable and well-monochromatized ($\Delta E_i \geq$ 2 keV) ^{15}N ion beam of 6-13 MeV. The authors have developed a computer control system for the accelerator to enable automated energy scanning and data acquisition for hydrogen profiling. Reflecting the two different NRA measurement tasks presented by the above H profiling applications, the MALT facility provides two ion beam lines with specialized experimental stations: (1) a UHV surface analytical system with a single bismuth germanate (BGO, $Bi_4Ge_3O_{12}$) γ-scintillation detector dedicated to the NRA quantitation of hydrogen surface coverages, to zero-point vibration spectroscopy, and to H depth profiling at atomically controlled single crystal targets in a unique combination with TDS; and (2) a high vacuum chamber equipped with two BGO detectors positioned very close to the target for increased γ-detection efficiency, providing for a lower H detection limit and faster data acquisition. This setup has no sample preparation facilities but allows for rapid sample exchange (~30 min) and thus for a higher throughput of targets for which a well-controlled surface layer is not an essential part of the analytical task, such as H profiling at buried interfaces or the quantitation of bulk H concentrations. At both beam lines, the BGO detectors are placed conveniently outside of the vacuum systems because the γ-rays penetrate the thin chamber walls with negligible attenuation.

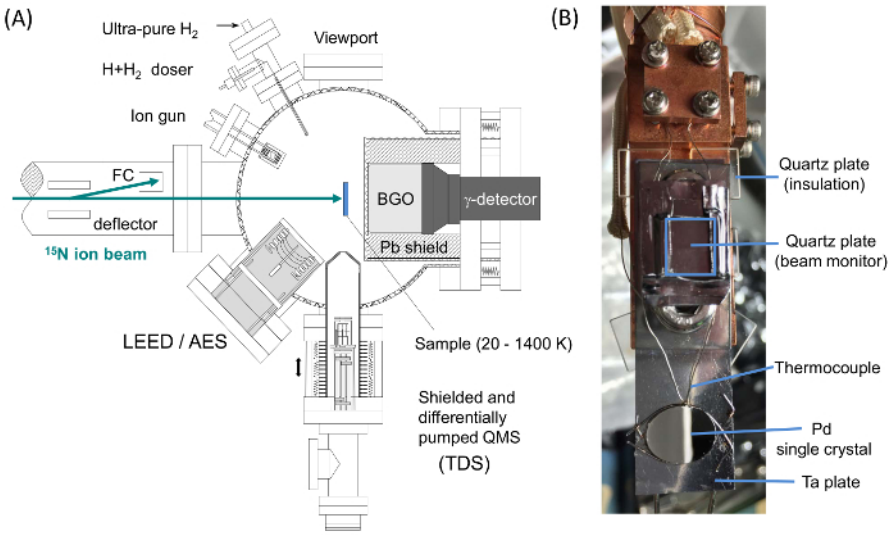

Figure 1. NRA setup in the BL-1E UHV system. (**A**) Schematic top view into the BL-1E UHV system equipped with sputter ion gun, low energy electron diffraction (LEED), and Auger electron spectroscopy (AES) for the *in-situ* preparation of atomically ordered and chemically clean single crystal surface targets and combined NRA and TDS measurements with a quadrupole mass spectrometer (QMS) mounted on a linear translation stage. (**B**) Pd single crystal specimen attached on the sample holder of the cryogenic manipulator. Please click here to view a larger version of this figure.

Figure 1 (A) illustrates the UHV system at beam line (BL)-1E, which is fully equipped for the *in-situ* preparation of atomically ordered single crystal surfaces and has a base pressure $<10^{-8}$ Pa to maintain surface cleanliness. To provide sample access for the surface-analytical tools, the 4" BGO scintillator is placed on the ^{15}N ion beam axis ~30 mm behind the target. The sample is mounted on a 4-axis manipulation stage for precise (x, y, z, Θ) positioning and can be cooled with liquid nitrogen to ~80 K or with compressed He to ~20 K. **Figure 1 (B)** shows a Pd single crystal target mounted by spot-welded Ta support wires to a He compression cryostat. Quartz sheet spacers insulate the sample holder plate electrically from the cryostat body. This enables the incident ^{15}N ion beam current measurement necessary for quantitative NRA and allows for electron bombardment heating from the tungsten filament on the backside of the sample holder. A type K thermocouple is spot-welded to the edge of the Pd specimen. A quartz plate attached on the manipulator axis above the sample is used to monitor the ion beam profile and for sample-beam alignment. **Figure 2 (A)** shows the setup at BL-2C with two 4" BGO detectors arranged at 90° with respect to the ^{15}N beam with their front face no further than 19.5 mm apart from the beam axis. The sample holder (**Figure 2 (B)**) provides a simple clamping mechanism for quick sample exchange and allows for rotation of the sample around the vertical axis to adjust the ^{15}N incidence angle.

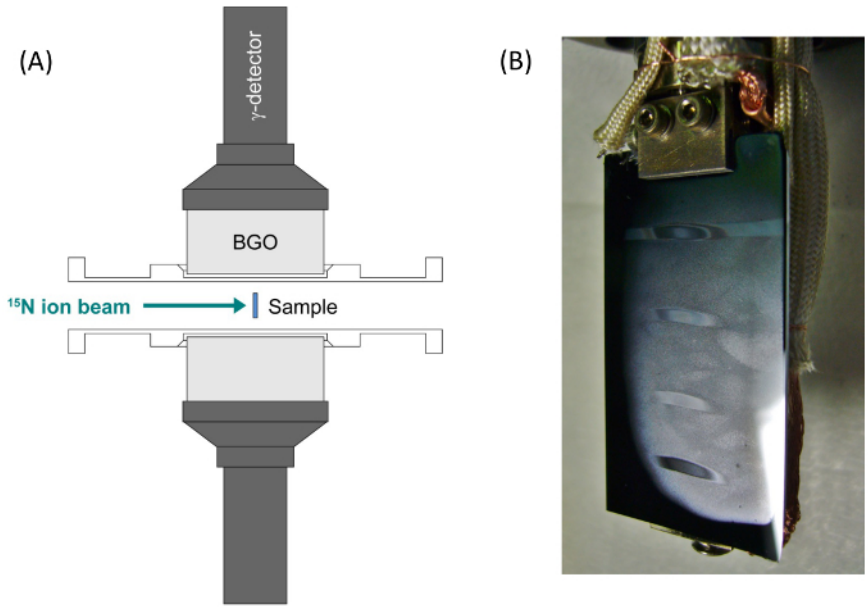

Figure 2. NRA setup at BL-2C. (**A**) Schematic top view into the high vacuum chamber at BL-2C equipped with two BGO γ-detectors close to the target position. (**B**) Sample holder with a large chip target of SiO_2/Si(100) clamped on. Fogging up this sample type with water vapor after the NRA analysis visualizes the spots that were irradiated by the ^{15}N ion beam. Please click here to view a larger version of this figure.

Protocol

1. Planning of Experiments

1. Identify the MALT accelerator beam line of interest depending on the measurement task (BL-1E for surface hydrogen, BL-2C for bulk or interfacial hydrogen). Contact the assisting scientist (currently M.W. or K.F.) to discuss details of the NRA measurements and their necessary preparations.
2. Download a beam time application form and observe the submission deadline on the MALT website[31].
   Note: The MALT facility invites new project proposals each March and September for the Summer (April-September) and Winter (October-March) half year terms, respectively.
3. Write the beam time proposal and submit as instructed on the MALT website.
4. After approval of the proposal, confirm the beam time schedule for the upcoming half year term as announced on the MALT website[31]. Safety training is required for new users in the beginning of the term.
5. Prepare for the beam time in advance. Consider all details of the experiment, and the time necessary for the transport of materials, for sample installation, and especially for *in-situ* surface preparation in UHV (if required). Ready the target specimen for the NRA measurement before the beam time starts.

2. Preparation for NRA Measurements at BL-1E (UHV)

Note: Always wear gloves when handling instruments and materials intended for use in vacuum, including the clean tools.

1. **Install single crystal sample into UHV (refer to Figure 1 (B)).**
   1. Set spot-welder power to 3.5. Place single crystal specimen onto clean, flat, non-conducting working surface and spot-weld two 4-cm long pieces of tantalum (Ta) wire (0.3 mm diam.) in parallel to sample edges.
   2. Gently bend wires to fit around the crystal edge shape while countering the bending forces with tweezers or pliers at the spot welding points. On a length of ~1 cm on each side, apply 2-4 additional spot welding points to the wire pair along the crystal edge.
   3. Bend wire ends to point away from crystal center in a horizontal plane parallel to the working surface. Place sample with support wires onto the Ta plate (0.3 mm thick) of the sample holder. Align sample to cover the hole above the backside filament heater and fix the specimen position by spot-welding all four support wire ends onto the plate. If possible, apply more than one welding point to each wire end, moving from wire tip towards sample.
   4. Cut away any excessive wire length standing out from holder plate edge. Set spot-welder power to minimum and release one pulse through spot-welding pliers closed empty. Spot-weld type K (chromel-alumel) thermocouple (0.2 mm diameter) to the upper edge of the crystal specimen.
   5. Confirm proper connectivity of the sample mount by measuring resistances between the electrical feedthrough contacts at the cryostat head: Filament vs. sample (bias contact wire attached to sample holder plate) > 20 MΩ; Filament vs. ground (cryostat body) > 20 MΩ; Filament leads (0.3 mm diam. W) < 3 Ω; Thermocouple leads: ~16 Ω; Thermocouple vs. ground > 20 MΩ; Thermocouple vs. sample ~20 Ω and ~8 Ω (depending on wire material, chromel or alumel).
   6. Note distance between centers of sample and beam profile monitor (quartz plate).
   7. Replace copper gasket on UHV manipulator head and carefully insert cryostat with mounted sample. Tighten flange bolts and evacuate UHV system following instructions from the assisting scientist.
   8. Prepare UHV chamber for bake out by attaching heater tapes and aluminum foil. Assure normal operation of all turbo-molecular pumps for at least 30 min and a pressure < 2×10^{-4} Pa. Turn on chamber heaters to bake the UHV system for 24 hr.
   9. Confirm ion gauge reading below 1×10^{-5} Pa. Turn off baking heaters. Reactivate non-evaporable getter (NEG) pump with internal heater element at 400-450 °C for 30 min while the chamber is still hot.
   10. Let chamber cool for 3-4 hr, then reattach QMS electronics and power supply cables to ion gun and LEED optics. Degas filaments of QMS, ion gun, and LEED. Confirm that chamber base pressure is <1×10^{-8} Pa after fully cooling to room temperature (within 12-24 hr).

2. **Prepare single crystal surface in UHV (refer to Figure 1 (A)).**
   1. Position sample in chamber center with the manipulator x, y, z-stage and rotate to align surface between viewport and ion gun (facing the gas doser). Switch on ion gun power supply and adjust 'Emission' control to 20 mA. Look at the sample through the viewport and fine-adjust sample rotation angle so that the mirror image of the glowing ion gun filament is visible on the sample surface.
   2. Set 'Beam energy' on ion gun power supply to 800 eV. Close NEG pump gate valve at the chamber bottom and introduce 6×10^{-3} Pa Ar gas into UHV chamber through variable leak valve. Confirm a sputter ion current (digital tester, from sample to ground) around 2 µA and sputter surface for 10 min at room temperature.
   3. Add liquid nitrogen to the manipulator cryostat. At manipulator head, connect filament heater leads to power supply and digital tester (20 mV range) to thermocouple feedthrough. Ground the filament.
   4. Connect sample contact to bias voltage power supply. Apply sample bias of 1 kV. Use filament heater currents up to 6.6 A for annealing, oxidation, and flash-heating in the next Step (2.2.5) while monitoring the thermocouple voltage (sample temperature) with the digital tester.
      CAUTION: NEVER touch digital tester or manipulator head while the sample is biased (risk of fatal electric shock!).
   5. Anneal sample in UHV to 1,000 K for 10 min ensuring the pressure remains below 2×10^{-7} Pa. Oxidize at 750 K in 5.0×10^{-5} Pa O_2 for 5 min, then reduce at room temperature (RT) in 5.0×10^{-5} Pa H_2. Perform a final flashing to 600 K in UHV.
   6. Observe LEED pattern and repeat Steps 2.2.1 to 2.2.2 (sputtering) and 2.2.3. to 2.2.5 (annealing/oxidation/H_2-reduction) until a clear (1×1) structure with bright spots on low background results (**Figure 3**) and no impurities remain in Auger electron spectroscopy[32]. Sputter for only 2-3 min in the repeated sputter/annealing cycles.
   7. (optional) Add liquid nitrogen to the manipulator cryostat to cool sample to 90 K and expose to a few Langmuirs (L) of H_2 gas (1 L = 1.33×10^{-4} Pa). Perform a TDS measurement and finally verify that the H_2 thermal desorption spectrum conforms with literature data[15].

Note: The preparations necessary in advance of the NRA beam time are now complete. The clean surface target can now be prepared routinely within ~2-3 hr by repeating Steps 2.2.1 through 2.2.6 with sputtering cycles of 2-3 min.

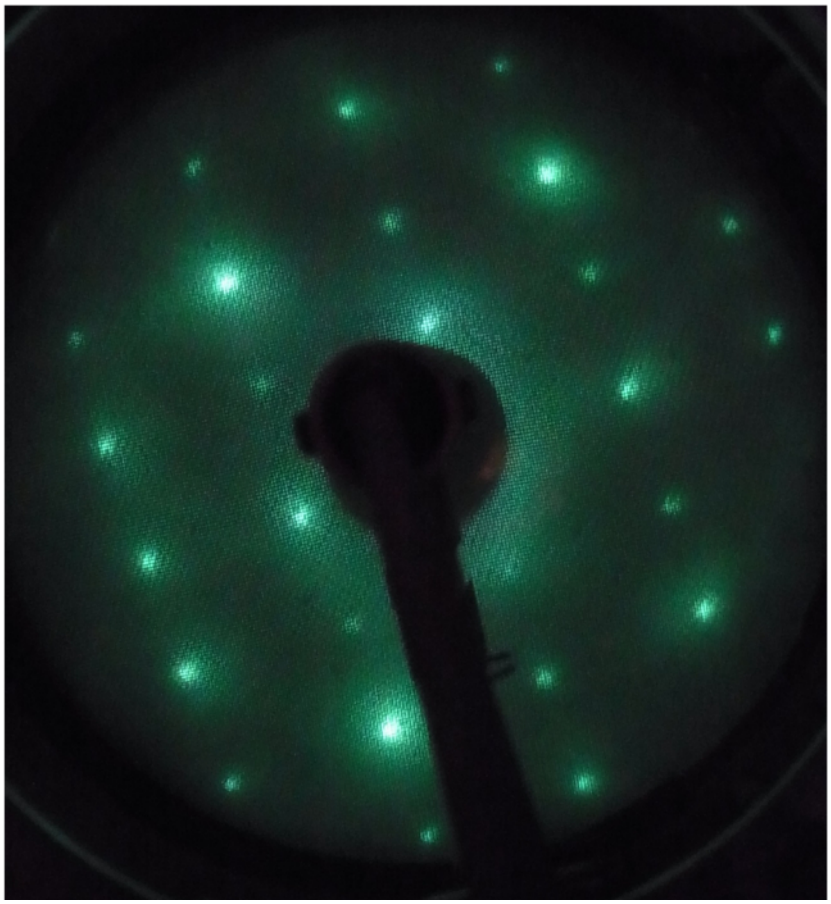

Figure 3. LEED pattern (223 eV) of the cleaned Pd(110) surface in the BL-1E UHV system. The clear (1×1) pattern with bright diffraction spots on a low background signifies an atomically well-ordered surface structure. Please click here to view a larger version of this figure.

3. Align ^{15}N ion beam to single crystal target.
    1. At the 1E UHV chamber, position sample in chamber center (x = 25, y = 26, adjust z by eye to height of QMS front aperture) and rotate to face ^{15}N ion beam line. Bring quartz plate beam profile monitor (**Figure 1 (B)**) into NRA measurement position by lowering sample holder by sample-monitor distance measured in Step 2.1.5. Set digital camera on window flange below the manipulator to transmit beam profile image on the quartz plate to the TV monitor in the accelerator control room.
    2. Remove all other electrical contacts to sample at manipulator head and connect signal line to digital current integrator in control room. Set electrostatic deflector voltage on BL-1E to 8,500 V. Open the three manual gate valves on BL-1E between the UHV chamber and the bending magnet BM04.
    3. Obtain instructions from the assisting scientist to become familiar with the accelerator control system in the control room.
    Note: Accelerator parameters (such as beam energy- and direction-defining magnet fields and focusing lenses) are set with assignable dials on a central control panel. Beam line valves and Faraday cups are remotely opened/closed by mouse clicks and pneumatic actuation.
    4. In the control room, switch current integrator from 'Stand by' mode to 'Operate'. Connect integrator analog output to current indicator. At the accelerator control panel, adjust ^{15}N ion beam energy with accelerator in slit feedback mode to an energy analyzer magnet field of 5,535 Gauss (Parameter: NMR03) and match bending magnet field (Parameter HPB04) to ~-6,033.4 Gauss to direct ion beam onto target in 1E UHV chamber. Set magnetic quadrupole lens parameters (MQ04) to XCC=4.64 A and YCC=5.15 A to focus beam approximately.
    5. In the control room, open two gate valves between accelerator and beam line 1E. Open Faraday cup (FC) FC04 and observe ion beam profile on quartz plate in target chamber on the TV monitor. Fine tune BM04 and MQ04 parameter settings to obtain well-focused ion beam in center of profile monitor plate. Adjust z-position of quartz monitor with sample manipulator if necessary.
    6. Close Faraday cup FC04 and lift up sample z-position again by sample-monitor distance. Take note of NMR03/HPB04/MQ04 (XCC, YCC) parameters and save them in a new MagparNNN.xls file for the current beam time (NNN, a three-digit number).
    Note: Based on this reference NMR03/HPB04 input, MagparNNN.xls calculates the matching magnet field parameters for the energy-analyzing (BM03) and direction-switching (BM04) magnets necessary to keep the ion beam position on the target during a ^{15}N energy scan.

3. Preparation for NRA Measurement at BL-2C

1. Lift up any previously used sample from the beam line position into to the manipulator transfer rod, secure height with fixation screw, and close gate valve to the beam line.
2. Detach sample current line at electrical feedthrough and rotary pump line at KF flange coupling of the manipulator. Detach manipulator from the gate valve flange.
3. Place manipulator onto preparation table and slide sample holder out of the transfer tube. Rotate manipulator axis to place sample horizontally.
4. Loosen two M2 cap screws of sample clamp (**Figure 2 (B)**) and remove old target. Set new sample, align parallel to manipulator axis, and tighten clamp screws. Retract sample into transfer tube and secure position with fixation screw.
5. Replace copper gasket on gate valve and reinstall manipulator on the beam line. Attach rotary pump line to manipulator. Close valve in the rotary pump line to the turbo-molecular pump (TMP).
6. Open rotary pump line valve of the manipulator and evacuate transfer tube for 10-15 min to restore rotary base pressure. Close manipulator pump line valves and open valve in rotary pump line to TMP. Slowly open the gate valve to the manipulator and evacuate for 20-30 min to restore 2-3×10^{-3} Pa.
7. Lower sample to beam line position and align surface normal of beam profile monitor (glass plate) to incident beam direction with aid of BL-2C camera and nearby TV monitor. Then connect BL-2C camera signal line to TV monitor in control room. Open two pneumatically actuated gate valves on BL-2C between the NRA chamber and bending magnet BM04.
8. Connect sample current signal line between electrical feedthrough of sample manipulator and digital current integrator (control room). In the accelerator control room, switch current integrator from 'Stand by' mode to 'Operate' and connect integrator analog output to current monitor.
9. Roughly align ^{15}N ion beam to target in BL-2C by setting bending magnet field (Parameter HPB04) to ~0.6 Gauss (Polarity: positive), magnetic quadrupole lens MQ04 parameters to XCC=4.64 A and YCC=5.15 A, and quadrupole lens MQ-2C parameters A=3.3 A and B=3.6 A to focus beam approximately.
10. Fine-tune HPB04/MQ04(XCC, YCC)/MQ-2C(A, B) parameters to optimize beam transmission (unobstructed passage to target) and beam profile on target (use beam profile monitors BPM-1C and BPM-2C and BL-2C camera image) and take note of the best settings.

4. NRA Measurement at BL-1E

1. Flash-heat Pd sample to 600 K to free surface from any adsorbed contaminants. Stabilize sample temperature at 145 K with filament heater (~3.6 A) and running He compression cryostat (or liquid nitrogen cooling).
2. Close valves to accelerator and to NEG pump and expose sample to 2,000 L H_2 (2.66×10^{-3} Pa × 100 sec) at 145 K. Let sample cool to 80 K and adjust a H_2 background pressure of 1×10^{-6} Pa.
3. In the control room, set ^{15}N ion beam energy at BM03 to desired start value for the energy scan (typically NMR03 = 5,525 Gauss) and adjust BM04 according to the MagparNNN.xls table.
4. Load the NRA data acquisition software (NRAmain.vi) on the accelerator control PC at BL-2C. Select depth profiling routine 'AutoScanLinuxUHVfb3.vi'. In AutoScanLinuxUHVfb3.vi, push 'Read present values' to transfer current magnet parameter settings to the control PC software.
5. Verify again that all valves on BL-1E are open, that the sample current signal line is connected, that the current digitizer is set to 'Operate', and that a ^{15}N beam of ideally 15±5 nA is available on FC04.
6. Set the stat START, STOP and STEP values of the BM03 parameter for the energy scan (typically 5,525 Gauss, 5,600 Gauss, and 1 Gauss, respectively) and turn the option 'Force TVC to gvm' on. For a ~15 nA beam of $^{15}N^{2+}$, set the 'Acquisition time' parameter to 50 sec.
7. Click the 'Execution' arrow in AutoScanLinuxUHVfb3.vi console to start automated acquisition of a depth profile (up to ~35 nm depth in Pd for STOP = 5,600 Gauss). At the end of the scan (or for an earlier termination), click 'Stop measurement' to close the data file.
8. Switch current digitizer to 'Stand by' mode, detach sample current line from sample manipulator feedthrough, and close the last gate valve on BL-1E before the UHV chamber.
9. Stop the background H_2 gas dosage by closing the variable leak valve. Open the NEG gate valve at the UHV chamber bottom. (Optional: Take a H_2 TDS spectrum of the sample.)
10. For additional NRA measurements (optional), re-expose the Pd(110) surface to H_2 as instructed in Step 4.2 and repeat Steps 4.3 through 4.9.

5. NRA Measurement at BL-2C

1. In the control room, set ^{15}N ion beam energy at BM03 to desired START value for the energy scan (typically NMR03 = 5,525 Gauss to start profiling at the surface).
2. Load the NRA data acquisition software (NRAmain.vi) on the accelerator control PC at BL-2C. Select depth profiling routine 'AutoScanLinux11.vi'. Enter the desired BM03 parameters for the automated energy scan (START, STOP, STEP), matching START to the BM03 value set in Step 5.1. For the present SiO_2/Si samples, set 'Acquisition time' to 50 sec.
3. Verify again that all valves on BL-2C are open, that the sample current signal line is connected, that the current digitizer is set to 'Operate', and that a $^{15}N^{2+}$ beam of 50-100 nA is available on FC04.
4. Click 'Execution' arrow in 'AutoScanLinux11.vi' to acquire a depth profile that terminates automatically at the STOP value of the BM03 parameter. At the end of the scan (or for earlier termination), click 'Stop measurement' to close the data file.

6. Data Analysis

1. Copy *.nra raw data files in /home/csadmin/DataTaking/BTNNN from the acquisition PC (NNN is the number of the current beam time) onto a USB memory stick and transfer to data analysis PC.
2. Start the home-built software package for NRA data analysis and open procedure 'NRA-Linux-2C-v3.ipf'. Obtain the procedures NRA-Analysis-2C-v4.ipf, LinuxAddOn-3-v3.ipf, and Menu-NRA.ipf and copy them to the data folder containing Igor User Routines.

3. Compile procedures and select 'Load NRA data' from the appearing 'NRA' menu. Select data file measured under Sections 4 or 5, and click 'Continue' in the appearing pop-up dialog.
   Note: The software generates two graph outputs from measured data: 'raw data' (raw γ-counts (*GRS*) vs. NMR03 magnet field as displayed during data acquisition), and 'NRA spectrum', corresponding to the excitation curve (background-subtracted and incident charge-normalized γ-yield (I_{norm}) vs. ^{15}N ion energy).
4. Select 'Correct Sample Current readings' from 'NRA' menu and choose the 'Recalculate ISC (entire wave) from averaged ISC/IFar ratio (*e.g.*, sample w/o bias)' option from the drop down menu to rescale ion beam charge reading from current digitizer to actual dimension (μC), referenced to the averaged FC04 beam current readings of the entire data set. Delete the 'Inorm_by_Faraday' trace from the 'NRA spectrum' graph.
   Note: Normalization to this scaled integrated incident charge is preferable (over normalization to the Faraday current) because it better reflects the ^{15}N ion charge that actually hits the target than the FC04 current. The latter is measured only once before the Faraday cup opens (to deliver the beam onto the target) and therefore does not account for beam current fluctuations that always occur to some degree during the acquisition time for each data point. Rescaling the sample charge is necessary because the current digitizer reading overestimates the actual incident ion beam charge due to secondary electron emission from the target.
5. Determine the NMR03 value corresponding to E_{res} (the maximum position of the surface resonance peak in the 'raw data' plot). If different from the software default value of 5,535 Gauss, correct the entry (if necessary also the Stopping power value) by selecting 'NMR, energy and depth scale' routine from the 'NRA' menu.
6. If a background rate (cps) correction has become necessary, use first the 'Correct Faraday readings' function to recalculate the normalized γ-yield from the raw (GRS) data after revising the background value, entering a correction factor of 1 (for the FC04 current). Then run the 'Correct Sample Current readings' function again (Step 6.4) to recalculate also the charge-normalized γ-yield with the revised background in properly scaled relation to the FC04 Faraday.
7. Plot charge-normalized γ-yield vs. depth as top axis to display the convolved hydrogen depth distribution (**Figure 4**).
8. Add error bars to the graph using the respective function from the 'NRA' menu. Whenever possible, prefer charge-normalization.
   Note: Counting statistics define the error Δ*I* of the NRA γ-yield, *I* = *GRS-Background*, through the error-propagated uncertainties of the measured raw counts, $\delta_{GRS} = \sqrt{GRS}$ and of the background, $\delta_{bg} = \sqrt{Background\ rate\ (cps)\ \times Acquisition\ time}$ hence calculates as: $\Delta I = \sqrt{(\delta_{GRS})^2 + (\delta_{bg})^2} = \sqrt{GRS + Background\ rate(cps) \times Acquisition\ time}$. The error bars in the depth profile graphs (**Figures 4** and **5**) are ΔI_{norm} = Δ*I*/incident ion beam charge.
9. (optional) Perform a fit analysis of the data with suitable model functions[3].

Representative Results

Figure 4 shows near-surface NRA H profiles of H_2-exposed Pd(110) measured in the BL-1E UHV system at a sample temperature of 90 K under a H_2 background pressure of 1.33×10^{-6} Pa. The ^{15}N ion incidence energy has been converted into probing depth using the stopping power of Pd (*S* = 3.90 keV/nm). The open symbol profile was obtained after pre-exposing the Pd(110) sample to 2,000 L H_2 at 145 K to induce absorption of hydrogen into the Pd bulk[15]. This profile can be decomposed into a peak at E_{res} = 6.385 MeV and a broad γ-yield plateau stretching over the entire profiled depth region. The peak at E_{res} corresponding to H on the target surface, whereas the plateau region proves that hydrogen absorption into the Pd bulk has taken place. The surface peak has a nearly Gaussian shape. To demonstrate this better, **Figure 4** includes two additional NRA excitation curves (gray and black solid symbols) that were recorded at 170 K under the same H_2 background pressure from a freshly prepared Pd(110) surface without H_2 pre-dosage. At this temperature only surface chemisorbed hydrogen is stable at Pd(110); any absorbed H would diffuse into the deeper bulk and escape from NRA detection in the near-surface region. Fitting the surface peak to a Gaussian profile yields a peak height of I_{max} = 86.9 ± 4.5 cts/μC and an: $FWHM = 2\sqrt{\ln(2)} \cdot \sigma$ of 11.6 ± 0.4 keV, where σ is the Gaussian width parameter. From the Gaussian peak area: $I_S = \sqrt{\pi} \cdot I_{max} \cdot \sigma$ and the γ-ray detection efficiency of the BGO background count rate (separate background measurements confirm that such random fluctuations occur) and stopping power of the BL-1E setup (calibrated with a Kapton $(C_{22}H_{10}O_5N_2)_n$ foil standard of precisely known H concentration (c_{bulk} = 2.28×10^{22} cm^{-3}) and stopping power *S* = 1.2879 keV/nm) α = 7.56×10^{-13} [(cts/μC) keV cm^2], one determines the absolute H density (N_s) on the H_2-exposed Pd(110) singe crystal as $N_s = I_S/\alpha = 1.42\times10^{15}$ cm^{-2}. Relative to the Pd atom density on the Pd(110) surface of 9.35×10^{14} cm^{-2} this corresponds to a H coverage of 1.52 ± 0.13 ML (monolayers), in very good agreement with the literature value (1.5 ML)[15,33,34].

Figure 4 also shows that the depth resolution of the NRA H profile in the near-surface region is limited by the width of the surface resonance peak to about 2-3 nm (≈FWHM/*S*). Therefore, any abrupt features in the H profile such as the point-to-point γ-yield variations seen around 16 nm depth cannot correspond to actually existing steep H concentration gradients, because such would be smeared out by the surface peak width and additional energy broadening due to ^{15}N ion straggling[3]. Hence, the γ-yield corrugations in the plateau region of the H profile (5 to 22 nm depth) reflect fluctuations of the BGO background count rate (separate background measurements confirm that such random fluctuations occur) and do not contain physical information on the depth distribution of the Pd-absorbed hydrogen. The latter distribution is expected to be rather smooth in the homogenous single crystal, where H diffusion is rapid (several 100 nm/sec even at 145 K)[3,13,15]. Thus, the approximately constant concentration of the bulk-absorbed hydrogen in the near-surface region of the Pd crystal after exposure to 2,000 L H_2 at 145 K can be evaluated by fitting the plateau data in **Figure 4** to a sigmoid function that rises to its half-height at E_{res} with the same width as the Gaussian surface peak[3]. This analysis determines the plateau height I_{bulk} to 15.4 ± 1.3 cts/μC. With the Pd stopping power *S* = 3.9 keV/nm, one thus obtains the H bulk concentration as $c_{bulk} = I_{bulk}S / \alpha = 7.94\times10^{20}$ cm^{-3}, or 1.2% of the atomic density in bulk Pd (the latter equation is also used to calibrate α after having measured I_{bulk} in the Kapton standard[3]). This bulk H concentration signifies that finely distributed grains of Pd hydride (which has a H/Pd ratio of about 0.65 at this temperature) has nucleated in the near-surface region of the Pd crystal during its exposure to 2,000 L (2.66×10^{-3} Pa × 100 sec) H_2 at 145 K, because the H solubility in the dilute solid solution phase of Pd amounts to less than H/Pd = 5×10^{-4} at this temperature and H_2 pressure.

Figure 5 displays ^{15}N NRA depth profiles from a series of SiO_2/Si(100) stacks as they can be measured at BL-2C. The SiO_2 films had thicknesses of 19.0, 30.0, and 41.5 nm[35]. In addition to a peak of surface hydrogen at E_{res}, all profiles show a second peak in larger depth, indicating that the H distribution within the oxide film is apparently not uniform. The position of this second peak shifts to larger depth with increasing SiO_2 film thickness. The optically determined SiO_2 film thickness is indicated by a vertical dashed line in each panel (i)-(iii). Close inspection reveals that the center positions of the NRA profile peaks are located with a small offset of ~4 nm above the respective SiO_2/Si interfaces. This evidences that hydrogen tends to accumulate not exactly at but in a region extending over a few nanometers of the oxide in front of the interface. This peculiar H localization behavior has been attributed to the near-interfacial SiO_2 structure, where a large number of strain and sub-oxide[36] related defects provide preferential binding sites for hydrogen species[37]. The strained interfacial region results from the reduction of the Si atom density by a factor of ~2 in the abrupt transition from crystalline Si to amorphous SiO_2. For quantitative evaluation the respective surface and near-interfacial peaks were fitted to Gaussian functions that are shown as solid lines in **Figure 5**. An analysis equivalent to the one described above for the surface H peak on Pd(100) reveals that the near-interfacial oxide regions of the SiO_2/Si(100) film stacks contained a H layer density of (1.0-1.3)×10^{14} cm^{-2}.

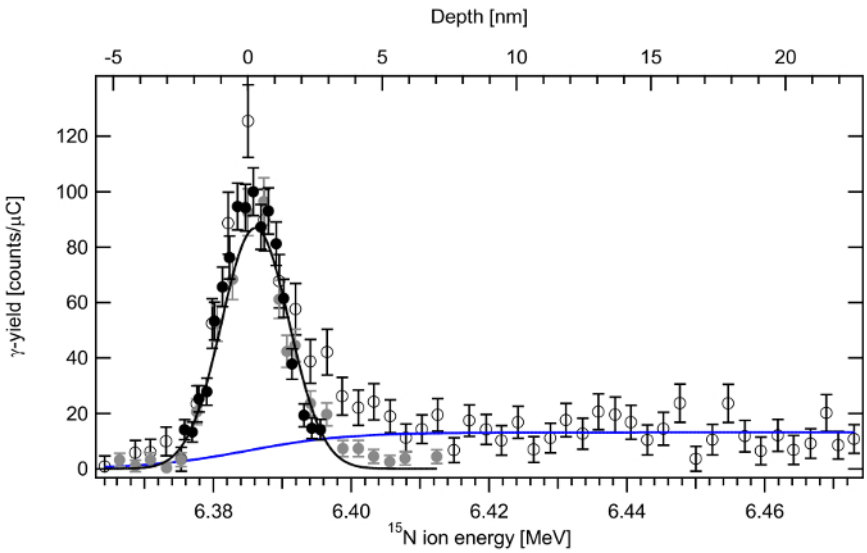

Figure 4. Near-surface NRA H profiles of Pd(110) obtained in the BL-1E UHV system under a H_2 background of 1.33×10^{-6} Pa. Open symbols: Pre-exposed to 2,000 L H_2 at 145 K, NRA measured at 90 K. Filled grey and black symbols: Two profiles measured at 170 K without H_2 pre-dosage. Refer to the Note in Procedure Step 6.8 for the error bar calculation. Please click here to view a larger version of this figure.

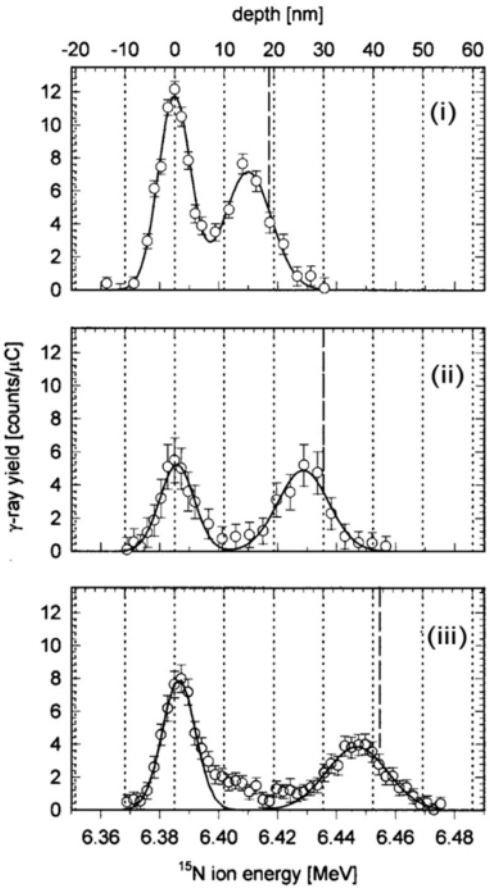

Figure 5. NRA H profile of three SiO_2 film on Si(100) measured in the BL-2C system. NRA H-profiles for three SiO_2 films on Si(100) with thicknesses of (i) 19.0 nm, (ii) 30.0 nm, and (iii) 41.5 nm. SiO_2/Si(100) interface positions are indicated by dashed vertical lines. This figure has been adapted from Ref. [35] with permission from AIP. Refer to the Note in Procedure Step 6.8 for the error bar calculation. Please click here to view a larger version of this figure.

Discussion

Figure 4 demonstrates the efficient distinction and quantitation of surface-adsorbed from bulk-absorbed hydrogen through ^{15}N NRA at the example of a Pd(110) single crystal in the BL-1E UHV system. The high reproducibility of the surface H peak in the three profiles attests to the reliability of the *in-situ* UHV sample preparation and to the non-destructive nature of the NRA measurement. The quantitative agreement of the determined H coverage with the expected atomic saturation density further shows the accuracy of the NRA measurement. Close comparison between the NRA profiles of H_2 pre-exposed Pd(110) (open symbols) and the two excitation curves of only surface hydrogen on Pd(110) (grey and black symbols) in **Figure 4** shows that the surface peak in the former H profile tails asymmetrically towards the plateau of bulk-absorbed hydrogen in the topmost ~5 nm. Such subtle detail of potentially non-uniform hydrogen distributions closely below the surface can only be revealed through NRA. A similar H accumulation in a shallow subsurface region has also been observed in other metals (Pt, Ti)[11,14]. The origin of this particular H behavior in the subsurface region is presently not clarified but scientifically interesting with regard to properly understanding the peculiar hydrogen absorption properties of nanomaterials[17] as opposed to extended bulk metals.

Several critical parameters should be observed in the Protocol in order to obtain high quality data such as those in **Figure 4**. The H_2 background pressure introduced in Step 4.2 (1×10^{-6} Pa) is a deliberate choice such as to stabilize the H-saturation coverage on the Pd surface by balancing NRA ion beam-induced H-desorption through H-readsorption from the H_2 gas on one hand, while at the same time avoiding H uptake into the Pd bulk by H_2 absorption, on the other. If the H_2 pressure was too high, H absorption during the NRA analysis would cause a gradual increase of the NRA signal at E_{res}, because the surface resonance peak overlaps with about 2 nm of the topmost Pd bulk region, where H may accumulate, especially at even lower temperatures than those in the experiments of **Figure 4**.[13-15,18] Thus, for H-absorbing materials such as Pd or Ti, the appropriateness of the H_2 background setting has to be verified by confirming that the γ-yield at E_{res} remains constant on the time scale required to measure the surface resonance profile. This complication does not arise for most materials that do not absorb hydrogen at low H_2 pressures. Here, quantitation of the surface H saturation coverage is easily performed after observing saturation of the γ-yield at E_{res} when the H_2 background pressure is stepwise increased (up to a maximum of 10^{-2} Pa tolerable by the vacuum pump system).

Observe further that the data in **Figure 4** were taken with a $^{15}N^{2+}$ beam current of 15±5 nA (Step 4.5). This beam current has proven to be sufficiently high, on one hand, as to develop reasonably intense γ-signals from the saturated layer density of surface H atoms from the viewpoint of acceptable data statistics and overall measurement time, and also to be still sufficiently gentle, on the other hand, as to avoid excessive H

desorption (which would again require higher H_2 background pressure for compensation) and sample heating (which may cause modification of the H depth distribution by thermal diffusion).

Although the NRA technique is versatile and easily applied to determine H surface layer densities on most vacuum compatible solid materials, limitations arise with respect to the detection of especially weakly adsorbed H-species that may not be stable against desorption under the incident ^{15}N ion beam irradiation even under loss-compensating H_2 gas background (< 10^{-2} Pa). For example, the authors have not yet succeeded in observing surface H-species with desorption temperatures (TDS) below ~70 K with NRA. The tendency of H to desorb from the sample or to redistribute inside the target by diffusion under the ion beam varies strongly between different target materials and should be evaluated as part of any given analysis by monitoring the γ-yield at the probing depth of interest as a function of the ion beam dose. Without a compensating H_2 background as applied here to Pd(110) where H readsorbs readily, in many cases a more or less pronounced exponential decay of the H-signal can be observed. Measuring and extrapolating such H-loss functions to zero ^{15}N exposure allows reproducing the original H density on or inside the target prior to perturbation by the ion beam (for details, see Ref. 3). If the target size permits, reducing the current density (nA/cm^2) in the beam-irradiated surface spot by defocusing the ion beam with aid of the MQ04 magnetic lenses (Protocol Steps 2.3.5 and 3.10) may alleviate H losses during the analysis. In general, excessive ^{15}N ion doses should be avoided as they may cause physical damage to the target surface in the form of defects, which can change the H adsorption (and absorption) properties. In case of single crystals, the LEED pattern of the surface and the shape of the H_2 TDS spectrum[15] should therefore be checked regularly. If any anomaly is observed, re-prepare the surface freshly as instructed (for Pd(110)) in Protocol Steps 2.2.1 through 2.2.6.

Figure 5 demonstrated at the example of thin film SiO_2/Si(100) stacks that hydrogen depth profiling analysis by ^{15}N NRA can straightforwardly determine the depth location of near-interfacial H layers and the H density therein without destroying the sample material. Note, however, that the H accumulation in the interfacial regions seen in the depth profiles may partially result from the NRA analysis itself, because the ^{15}N ion irradiation can cause redistribution of hydrogen in the material. This is a well-known effect[35,38-40] and any possible H relocation during the NRA analysis should be verified by measuring the H concentration evolution at the accumulation peak depth on a non-irradiated sample spot in the course of continued ^{15}N ion irradiation. Although this beam-induced H relocation effect can make determining the original H distribution in a specimen somewhat more difficult, it can be exploited for analytical purposes in dielectric reliability research to evaluate H redistribution trends between intact interfaces of (model) MOS device structures, providing information on relative material-specific H mobilities.[3,26]

Regarding the H detection limit of the NRA measurement, we note that the setup in BL-2C with its larger BGO detection solid angle (**Figure 2 (A)** has a more than twice as large calibrated γ-detection efficiency factor (α_{2C} = 1.79×10^{-19} (cts/μC) (keV/nm) cm^3) as in BL-1E (α_{1E} = 7.56×10^{-20} (cts/μC) (keV/nm) cm^3)) and hence provides higher sensitivity, favorable for the measurement of low H concentrations in materials that do not require *in-situ* surface preparation. The background count rate in our γ-detection system is currently ~0.1 cps, setting a detection limit for volume H concentrations in solids in the order of 100 ppm (several 10^{18} cm^{-3}) with a 100-nA beam of $^{15}N^{2+}$ at BL-2C. In the present examples, this increased sensitivity (in combination with a stronger ion beam), permitted measuring the surface and interfacial layer H densities in the SiO_2/Si stacks with the same acquisition time (50 sec) as the about one order of magnitude larger surface H saturation layer on Pd(110) (compare vertical axis scales in **Figures 4** and **5**). The required acquisition time is determined by the desired counting statistics, the given H density in, and the ^{15}N ion beam current tolerated by the target. The acquisition time also defines the time resolution for the observation of transiently evolving H densities such as upon adsorption, desorption, absorption, or diffusion of hydrogen on or in materials.

The higher vacuum base pressure at BL-2C (~1×10^{-5} Pa) may cause deposition of H-containing contaminants from the residual gas onto the target surface during the NRA measurement[41]. This may result in large surface H peaks in the depth profiles that can overwhelm features of interest directly below the surface, similar (but worse than) as seen, *e.g.*, in the overlap with the shallower SiO_2/Si interfacial peak in **Figure 5 (i)**. A large H content in the surface layer also negatively affects the evaluation of small bulk H concentrations in large probing depths (E_i > ~9 MeV) by inducing γ-ray background due to non-resonant nuclear reaction yield[42]. Although the BL-2C system presently already features 10-cm thick lead (Pb) shielding blocks for the BGO detectors (not shown for clarity in **Figure 2**) that reduce the count rate of environmental γ-radiation background, further improvement of the H detection limit may be achieved by implementing anti-coincidence shielding for the detectors, which can reduce background signals due to highly penetrating cosmic muon radiation[43].

Disclosures

The authors declare that they have no competing financial interests.

Acknowledgements

We greatly appreciate M. Matsumoto for implementing the software that enables the automated measurement of NRA H depth profiles by remotely controlling the MALT accelerator parameters from the data acquisition PC. We thank K. Namba for skillfully performing Pd(110) sample preparations and NRA and TDS measurements at the BL-1E UHV system, and C. Nakano for technical assistance in the accelerator operation. The SiO_2/Si(100) specimen is gratefully received as a courtesy of Z. Liu of NEC Corporation, Japan. This work is partially supported by Grants-in-Aid for Scientific Research (Grant numbers 24246013 and 26108705) of the Japan Society for the Promotion of Science (JSPS), as well as through a Grant-in-Aid for Scientific Research in Innovative Areas 'Material Design through Computics: Complex Correlation and Non-Equilibrium Dynamics' from the Ministry of Education, Culture, Sports, Science, and Technology of Japan.

References

1. Lanford, W. A. Analysis for hydrogen by nuclear-reaction and energy recoil detection. *Nucl. Instrum. Methods Phys. Res. B.* **66** (1-2), 65-82, (1992).
2. Lanford, W. A. Nuclear Reactions for Hydrogen Analysis. In: *Handbook of Modern Ion Beam Materials Analysis.* Tesmer, J. R., & Nastasi, M., eds., Chapter 8, 193-204, Materials Research Society, Pittsburgh, PA, (1995).

3. Wilde, M., & Fukutani, K. Hydrogen detection near surfaces and shallow interfaces with resonant nuclear reaction analysis. *Surf. Sci. Rep.* **69** (4), 196-295, (2014).
4. Lanford, W. A., Trautvetter, H. P., Ziegler, J. F., & Keller, J. New precision technique for measuring concentration versus depth of hydrogen in solids. *Appl. Phys. Lett.* **28** (9), 566-568, (1976).
5. Ross, R. C., Tsong, I. S. T., Messier, R., Lanford, W. A., & Burman, C. Quantification of hydrogen in a-Si-H films by IR spectrometry, N-15 nuclear-reaction, and SIMS. *J. Vac. Sci. Technol.* **20** (3), 406-409, (1982).
6. Suzuki, T., Konishi, J., Yamamoto, K., Ogura, S., & Fukutani, K. Practical IR extinction coefficients of water in soda lime aluminosilicate glasses determined by nuclear reaction analysis. *J. Non-Cryst. Solids.* **382** (0), 66-69, (2013).
7. Wagner, W., Rauch, F., & Bange, K. Concentration profiles of hydrogen in technical oxidic thin-films and multilayer systems. *Fresenius Z. Analyt. Chem.* **333** (4-5), 478-480, (1989).
8. Wagner, W., Rauch, F., Ottermann, C., & Bange, K. In-depth profiling of hydrogen in oxidic multilayer systems. *Surf. Interf. Anal.* **16** (1-12), 331-334, (1990).
9. Wagner, W., Rauch, F., Ottermann, C., & Bange, K. Hydrogen dynamics in electrochromic multilayer systems investigated by the N-15 technique. *Nucl. Instrum. Methods Phys. Res. B.* **50** (1-4), 27-30, (1990).
10. Hjörvarsson, B., Rydén, J., Karlsson, E., Birch, J., & Sundgren, J. E. Interface effects of hydrogen uptake in Mo/V single-crystal superlattices. *Phys. Rev. B.* **43** (8), 6440-6445, (1991).
11. Fukutani, K., Itoh, A., Wilde, M., & Matsumoto, M. Zero-Point Vibration of Hydrogen Adsorbed on Si and Pt Surfaces. *Phys. Rev. Lett.* **88** (11), 116101, (2002).
12. Ericson, J. E., Dersch, O., & Rauch, F. Quartz hydration dating. *J. Archaeological Sci.* **31** (7), 883-902, (2004).
13. Wilde, M., Matsumoto, M., Fukutani, K., & Aruga, T. Depth-resolved analysis of subsurface hydrogen absorbed by Pd(100). *Surf. Sci.* **482-485** (Part 1), 346-352, (2001).
14. Wilde, M. *et al.* Hydrogen sorption by Ti(0001) single crystal surfaces. *J. Vac. Soc. Jpn.* **45** (5), 458-462, (2002).
15. Ohno, S., Wilde, M., & Fukutani, K. Novel insight into the hydrogen absorption mechanism at the Pd(110) surface. *J. Chem. Phys.* **140** (13), 134705, (2014).
16. Fukutani, K., Wilde, M., & Matsumoto, M. Nuclear-reaction analysis of H at the Pb/Si(111) inter-face: Monolayer depth distinction and interface structure. *Phys. Rev. B.* **64** (24), 245411, (2001).
17. Wilde, M., Fukutani, K., Naschitzki, M., & Freund, H. J. Hydrogen absorption in oxide-supported palladium nanocrystals. *Phys. Rev. B.* **77** (11), 113412, (2008).
18. Wilde, M., & Fukutani, K. Penetration mechanisms of surface-adsorbed hydrogen atoms into bulk metals: Experiment and model. *Phys. Rev. B.* **78** (11), 115411, (2008).
19. Okada, M., Nakamura, M., Moritani, K., & Kasai, T. Dissociative adsorption of hydrogen on thin Au films grown on Ir(111). *Surf. Sci.* **523** (3), 218-230, (2003).
20. Okada, M. *et al.* Reactivity of gold thin films grown on iridium: Hydrogen dissociation. *Appl. Catal. A General.* **291** (1-2), 55-61, (2005).
21. Okada, M. *et al.* Reactive gold thin films grown on iridium. *Appl. Surf. Sci.* **246** (1-3), 68-71, (2005).
22. Ogura, S. *et al.* Hydrogen adsorption on Ag and Au monolayers grown on Pt(111). *Surf. Sci.* **566-568** (Part 2), 755-760, (2004).
23. Fukutani, K. *et al.* Interface hydrogen between a Pb overlayer and H-saturated Si(111) studied by a resonant nuclear reaction. *Surf. Sci.* **377** (1-3), 1010-1014, (1997).
24. Fukutani, K., Iwai, H., Murata, Y., & Yamashita, H. Hydrogen at the surface and interface of metals on Si(111). *Phys. Rev. B.* **59** (20), 13020-13025, (1999).
25. Wilde, M., & Fukutani, K. Low-temperature growth of Au on H-terminated Si(111): Instability of hydrogen at the Au/Si interface revealed by non-destructive ultra-shallow H-depth profiling. *Jpn. J. Appl. Phys.* **42** (7B), 4650-4654, (2003).
26. Liu, Z., Fujieda, S., Ishigaki, H., Wilde, M., & Fukutani, K. Current Understanding of the Transport Behavior of Hydrogen Species in MOS Stacks and Their Relation to Reliability Degradation. *ECS Transactions.* **35** (4), 55-72, (2011).
27. Zinke-Allmang, M., & Kalbitzer, S. A novel method to determine vibrational energy states of atomic systems. *Z. Physik A.* **323** (2), 251-252, (1986).
28. Zinke-Allmang, M., Kalbitzer, S., & Weiser, M. Nuclear reaction spectroscopy of vibrational modes of solids. *Z. Physik A.* **325** (2), 183-191, (1986).
29. Bohr, N. *K. Dan. Vidensk. Selsk. Mat.-Fys. Medd.* **18** (1948).
30. Rud, N., Bøttiger, J., & Jensen, P. S. Measurements of energy-loss distributions for 6.5 MeV ^{15}N ions in solids. *Nucl. Instrum. Methods.* **151** (1-2), 247-252, (1978).
31. *MALT.* <http://malt.n.t.u-tokyo.ac.jp/index.html> (2015).
32. Briggs, D., & Seah, M. P. *Practical Surface Analysis by Auger and X-ray Photoelectron Spectroscopy.* John Wiley & Sons, Chichester, (1983).
33. Rieder, K. H., Baumberger, M., & Stocker, W. Selective Transition of Chemisorbed Hydrogen to Subsurface Sites on Pd(110). *Phys. Rev. Lett.* **51** (19), 1799-1802, (1983).
34. Dong, W., Ledentu, V., Sautet, P., Kresse, G., & Hafner, J. A theoretical study of the H-induced reconstructions of the Pd(110) surface. *Surf. Sci.* **377 - 379** (0), 56-61, (1997).
35. Wilde, M. *et al.* Influence of H_2-annealing on the hydrogen distribution near SiO_2/Si(100) interfaces revealed by in situ nuclear reaction analysis. *J. Appl. Phys.* **92** (8), 4320-4329, (2002).
36. Himpsel, F. J., McFeely, F. R., Taleb-Ibrahimi, A., Yarmoff, J. A., & Hollinger, G. Microscopic structure of the SiO_2/Si interface. *Phys. Rev. B.* **38** (9), 6084-6096, (1997).
37. Helms, C. R., & Poindexter, E. H. The silicon-silicon dioxide system: Its microstructure and imperfections. *Rep. Progr. Phys.* **57** (8), 791, (1994).
38. Briere, M. A., Wulf, F., & Braunig, D. Measurements of the accumulation of hydrogen at the silicon-silicon-dioxide interface using nuclear reaction analysis. *Nucl. Instrum. Methods Phys. Res. B:.* **45** (1-4), 45-48, (1990).
39. Ecker, K. H., Krauser, J., Weidinger, A., Weise, H. P., & Maser, K. Nuclear reaction analysis of hydrogen migration in silicon dioxide films on silicon under N-15 ion irradiation. *Nucl. Instrum. Methods Phys. Res. B.* **161-163** (0), 682-685, (2000).
40. Maser, K. *et al.* Hydrogen migration in wet-thermally grown silicon dioxide layers due to high dose ^{15}N ion beam irradiation. *Microelectron. Eng.* **48** (1-4), 139-142, (1999).
41. Bugeat, J. P., & Ligeon, E. Influence of ion beam bombardment in hydrogen surface layer analysis. *Nucl. Instrum. Methods.* **159** (1), 117-124, (1979).

42. Wilde, M., & Fukutani, K. Evaluation of non-resonant background in hydrogen depth profiling via $^{1}H(^{15}N,ag)^{12}C$ nuclear reaction analysis near 13.35 MeV. *Nucl. Instrum. Methods Phys. Res. B.* **232** (1-4), 280-284,(2005).
43. Horn, K. M., & Lanford, W. A. Suppression of background radiation in BGO and NaI detectors used in nuclear reaction analysis. *Nucl. Instrum. Methods Phys. Res. B.* **45** (1-4), 256-259, (1990).

